Photocatalysis of Ag-loaded $MgTiO_3$ for degradation of Fuchsin dye and dyes present in textile wastewater under sunlight

Dissertation submitted in partial fulfillment of

the requirements for the award of degree of

Master of Science

in **Chemistry**

Submitted by: VISHAL TIWARI

Registration no.: 302202013

Under the guidance of

Dr. Bonamali Pal

Professor

Dr. Satnam Singh

Professor

THAPAR INSTITUTE
OF ENGINEERING & TECHNOLOGY
(Deemed to be University)

Department of Chemistry and Biochemistry
Thapar Institute of Engineering and Technology
Patiala-147004, Punjab, India

DECLARATION

I hereby declare that the dissertation, "**Photocatalysis of Ag-loaded $MgTiO_3$ for degradation of Fuchsin dye and dyes present in textile wastewater under sunlight**," submitted to the Department of Chemistry and Biochemistry, Thapar Institute of Engineering and Technology, Patiala, in partial fulfillment of the requirements for the award of a Master of Science in Chemistry, is a record of my work that I conducted from January 2024 to July 2024 under the supervision of Dr. Bonamali Pal and Dr. Satnam Singh. The results contained in this dissertation have not been submitted in part or full to any other university or institute for the award of any other degree or diploma.

Tiwari

(Vishal Tiwari)

Date: 30-7-2024

Place: Patiala

Registration Number - 302202013

CERTIFICATE

This is to certify that the dissertation entitled **"Photocatalysis of Ag-loaded $MgTiO_3$ for degradation of Fuchsin dye and dyes present in textile wastewater under sunlight"** being submitted by **Vishal Tiwari** to the **Department of Chemistry and Biochemistry, Thapar Institute of Engineering and Technology, Patiala,** in partial fulfillment of the requirements for the award of degree of the **Master of Science in Chemistry,** is an authentic record of the work carried out by the candidate under our guidance and supervision. He has fulfilled the requirements for the submission of this dissertation, which, to our knowledge, has reached the requisite standard.

The results embodied in the dissertation have not been submitted in part or full to any other university or institute for the award of any other degree or diploma.

Date: 30/07/2024

Place: Patiala

Dr. Bonamali Pal

Professor

Dr. Satnam Singh

Professor

ACKNOWLEDGMENTS

I would not have been able to complete this M.Sc. project without the assistance and advice I received from numerous individuals, and it has been a truly life-changing experience for me.

First and foremost, I would like to express my sincere gratitude to my supervisors, **Dr. Bonamali Pal** and **Dr. Satnam Singh**, for all of their support and inspiration. They have consistently offered technical materials, and we have had insightful discussions about the given topic, for which I am grateful. Without their inspiration and assistance, this accomplishment would not be complete.

I would like to express my gratitude to the **Department of Chemistry and Biochemistry at Thapar Institute of Engineering and Technology** for their invaluable help during this project. The kind help from the DST-FIST program for HRMS analysis (**SR/FST/CS-II/2018/69**). I would also like to express gratitude to DBT (**BT/PR36172/NNT28/1811/2021**), the CSIR project under the scheme **(No.1(3082)/21/EMR-II),** and the DST-PURSE program (SR/PURSE/2023/213) for research equipment.

I would like to express my gratitude to **Ms. Sukhandeep Kaur**, my lab research scholar, for her patience, guidance, and sharing of her experience. Without her, this accomplishment would not have been possible.

Lastly, I would like to express my gratitude to my parents, in particular to my mother and father, for their unwavering and unselfish support in all aspects of my life—from moral to financial—during my dissertation and the years I spent studying.

Date:30/07/2024

Place: Patiala

Tiwari

Vishal Tiwari

ABSTRACT

Our research focuses on the fabrication of $MgTiO_3$ by a sonochemical approach and improving its photocatalytic characteristics by loading it with Ag metal. This change allows the photocatalyst to efficiently absorb broad-spectrum solar light while also effectively separating charges, which are critical for photocatalysis. Both $MgTiO_3$ and Ag-$MgTiO_3$ were discovered to exhibit spherical shapes, with Ag showing as smaller spheres and $MgTiO_3$ as bigger ones. The Ag-$MgTiO_3$ photocatalyst effectively degraded Fuchsin dye (Fuc) under solar light exposure, achieving a rate constant of 0.0314 min^{-1} over 50 minutes. Comparable tests with visible and UV light produced lower Fuc breakdown rates of 87% and 62.3%, respectively, highlighting direct sunlight as our catalyst's most effective light source (99.2%). Even at low concentrations (0.3 g/L), Ag-$MgTiO_3$ demonstrated excellent efficiency. Its photocatalytic activity substantially outperformed typical market options for TiO_2-P25 powder, which only achieved 42% removal of fuc dye. The catalyst had a zero charge surface pH of 4.46 and achieved maximum Fuc decomposition efficiency at pH 7. Reusability experiments showed the catalyst's high stability, with an 81.8% Fuc degradation efficiency after five repetitions. Scavenger studies emphasized the crucial role of $O_2^{\bullet-}$ active species in the photodecomposition process, including DMSO, a marked alteration lowering Fuc degradation effectiveness to 37.5 percent. Additionally, Ag-$MgTiO_3$ showed a remarkable 67.8% reduction in total organic carbon (TOC) for Fuc Dye. HRMS demonstrated the formation of simpler intermediates during contaminant degradation. Ag-$MgTiO_3$, with its simple synthesis method and outstanding performance, is a promising alternative for eliminating persistent pollutants in textile wastewater systems.

Keywords: Ag loaded $MgTiO_3$ photocatalyst; Photocatalytic activity of Ag-$MgTiO_3$; Photodegradation of Fuchsin dye; Textile dye degradation; Visible/Sunlight irradiation

TABLE OF CONTENTS

LIST OF ABBREVIATIONS

Fuc: Fuchsin dye

DI: distilled water

wt%: weight percentage

NCs: nanocomposites

VB: valence band

CB: conduction band

Eg: band gap

LSPR: Localized surface plasmon resonance

XRD: X-ray diffraction

FE-SEM: Field Emission scanning electron microscope

EDS: Energy-dispersive X-ray spectroscopy

DRS: UV-visible diffuse reflectance spectroscopy

PL: photo-luminescence

XPS: X-ray photoelectron spectroscopy

TOC: Total Organic Carbon

HR-TEM: High-resolution Transmission Electron Microscopy micrographs

LIST OF SYMBOLS

°C: degree Celsius

%: percentage

k: rate constant

a.u.: arbitrary unit

rpm: revolution per minute

eV: electron volt

mg: milligram

1. INTRODUCTION AND LITERATURE REVIEW

1.1 Introduction

The expanding demands on the world's energy supply and the damaging consequences of environmental contamination have emerged as humanity's top concerns.[1,2] As industrialization progresses, pollutants like pesticides, heavy metals, organic compounds, synthetic dyes, pharmaceutical residues, and other dangerous chemicals are being released at an unprecedented rate, seriously contaminating water supplies.[3–5] An astounding 43,000 tons of organic colorant are fabricated annually, and unfortunately, over 10% of this quantity ends up in our priceless water bodies [6]. Synthetic dyes, which we frequently use daily, significantly contribute to environmental contamination. Azo dyes are among the most dangerous types of artificial colors. Its discharge through textile industry wastewater must be taken severely because of its rich chemical composition, which includes amino groups, aromatic rings, and azoic linkages. As a result, they are potent pollutants in the aquatic environment. Specifically, the synthetic dyes released into the effluent exhibit a high degree of resistance to the usual water remediation methods, including chemical remediation, adsorption, membrane filtration, electrolytic removal, ozone processing, and other methods [7,8].

Semiconductor-based photocatalysis is one of the most enticing modern oxidation methods for cleaning wastewater. Its advantages include its simplicity, effectiveness, and environmental friendliness. In essence, energy-rich photons are absorbed, equivalent to or greater than the semiconductor's band gap, to create electron-hole pairs, which subsequently combine with hydroxyl and oxygen species to produce active ions capable of swiftly and efficiently breaking down the pollutants in the water [9,10]. Numerous semiconductor technologies and their composite materials have been designed and explored in great detail thus far in this area. Perovskite oxides in the form of ABO_3 are among the many catalytic materials that have been studied to date, and they are attracting much interest due to their enormous potential in various applications [11,12]. Perovskite oxides have been the subject of extensive research owing to their exceptional physical-chemical and optoelectronic features, encompassing great heat-related and photo-corrosion durability, electron conductivity, economical manufacturing expense, and structural flexibility [13].

Under sunlight irradiation, photocatalysis breaks down organic contaminants into simpler substances like water (H_2O) and carbon dioxide (CO_2) [14]. Numerous semiconductor materials have been investigated for their potential as a viable photocatalyst for eliminating ecological contaminants in

the presence of sunlight. Among them, one effective photocatalyst is $MgTiO_3$, a perovskite metal oxide. The layered structure of $MgTiO_3$ allows for improved charge separation, and it also has strong chemical and thermal stability, producing a high level of photocatalysis [15]. Apart from its photocatalytic function, this substance has wide-ranging uses in communication antennas and global position systems operating on microwave radiation [16,17].

To synthesize $MgTiO_3$ nanoparticles, several techniques have been used, including sol-gel, co-precipitation, metal-organic, solid-state processes, and hydrothermal mechano-chemical complexation approaches [18–20]. In general, two phases make up $MgTiO_3$: $MgTi_2O_5$ and Mg_2TiO_4. The current investigation utilized the sonochemical approach to successfully manufacture $MgTiO_3$ nanoparticles without needing these two phases. The use of ultrasound in research has grown recently due to the peculiar qualities of the product created by the sonochemical process, which set it apart from other methods. This is because tiny particles with a large surface area are created using ultrasound. In addition, this process produces nanoparticles and may react quickly with high purity and adjustable reaction conditions [21,22].

The effectiveness of the synthesized nanocomposite was next evaluated concerning the degradation of a colored pollutant (fuchsin dye) and wastewater that we took from a textile dyer in Model Town, Patiala, using solar light. A thorough series of tests were carried out, including the refinement of metal-loaded $MgTiO_3$ concentration, reaction kinetic analysis, pH influence, recyclability assessment, and active species detection tests.

Plasmonic metal nanoparticles (Ag, Au, Cu, Pt) can potentially improve the photocatalytic efficiency of SCs. Plasmonic metal nanoparticles (NPs) have exceptional localized surface plasmon resonance (LSPR) properties that enhance the spectral behavior of the visible region by creating excited electrons, producing more radicals, and increasing the separation of charge carriers [23]. Furthermore, due to a Schottky barrier at the M-SC junction, these metal nanoparticles can operate as electron trap sites, catching the high-energy electrons flowing from the $MgTiO_3$ Conduction Band. This significantly speeds up the separation of electron-hole pairs, contributing to the enhancement [24]. A. Shawky et al. produced Pt-decorated $CaTiO_3$ nanocrystals with different Pt loadings and tested their photoreduction of nitrobenzene to aniline. Pt deposition boosted the conversion rate significantly [25]. Zhen et al. fabricated Ag/α-MoO_3 heterojunctions that facilitate the removal of thiophene by nearly 2.5 times compared to bare α-MoO_3 [26]. Similarly, Au/ZnTiO3 nanocomposites demonstrated an incredible increase in the H_2 evolution rate under UV and visible light. Silver has been identified as a leading candidate for producing plasmonic photocatalytic materials because of

its minimal cost, excellent electrical conductance, and significant Localized surface plasmon resonance effect [27].

Numerous observations in the literature indicate that metal deposition significantly enhances the photocatalytic activity of the material when exposed to visible illumination. Thus, decorating $MgTiO_3$ surfaces with metals enhances their photocatalytic activity.

The report examines the photocatalytic performance of Ag-modified $MgTiO_3$ nanocomposites (containing 1 wt% Ag). The sonochemical method was used to produce the photocatalyst $MgTiO_3$, and subsequently, Ag was deposited on it using the photo-deposition process. Due to its availability, low cost, and acceptable redox potential (Ag = 0.799 V) to the conduction band of $MgTiO_3$, The synthesized sample was then characterized using various approaches and assessed for photocatalytic performance by removing fuchsin dye under sunlight. Individual studies examined the impact of Ag loading on light absorption and photocatalytic activity.

1.2 Objectives

1) Preparation and characterization of $MgTiO_3$ and the photo deposition of noble metal Ag on it.
2) To study the various physiochemical properties of Ag-modified $MgTiO_3$ nanocomposites.
3) To study the photocatalytic degradation of fuchsine dye and dyes in textile wastewater by Ag-$MgTiO_3$ nanocomposites under visible illumination and solar light.

2. EXPERIMENTAL SECTION

2.1. Apparatus

Measuring cylinders, Beakers, Conical flask, volumetric flask, Magnetic Stirrer, Glass Vials, Droppers, Petri dishes, Spatula, Magnetic beads, Test tubes, thermometer, crucible, weighing balance, centrifugation tubes, and pH paper were used.

2.2 Chemicals and Reagents

Potassium Hydroxide Pellets (85%), Nitric Acid (69%), isopropyl alcohol (98%), Magnesium nitrate hexahydrate (98%), ethanol (C_2H_5OH, 99.9%) were purchased from Loba Chemie, india. Titanium dioxide (P_25-TiO_2) was obtained from Degussa Corporation. Silver nitrate ($AgNO_3$) was purchased from Sigma-Aldrich (India), and Fuchsin dye (Pulver) was bought from MERCK DARMSTADT, Germany. Double distilled water from Organo Biotech Laboratories Pvt. Ltd.

2.3 Synthesis of $MgTiO_3$ nanocomposite

Scheme 1 depicts the flowchart that illustrates the experimental procedure of the preparation method. After being dissolved in 60 ml of 1M nitric acid, 1g of TiO_2 was subjected to a 15-minute sonication. Concurrently, a $Mg(NO_3)_2$ solution was made, which involved dissolving 2.5 g of $Mg(NO_3)_2 \cdot 6H_2O$ in 10 mL of double-deionized water, mixing it with the sonicated solution and then sonicating it for an additional 15 minutes. Following sonication, a further two hours of sonication were performed after adding 3M KOH solution using a dropper to get the pH down to 12. Following the reaction's conclusion, the precipitate was recovered using centrifugation, repeatedly cleaned with double-deionized water to remove contaminants, and rinsed with ethanol. The final product was obtained by drying the precipitate at 100 ^{0}C for 4 hours and calcining it for 2 hours at 700 ^{0}C after washing.

2.4 Synthesis of Ag-modified $MgTiO_3$

Scheme 2 shows the technique used to carry out the photo deposition of Ag on the $MgTiO_3$ surface. In separate test tubes with deionized water and isopropyl alcohol as a hole absorber (5 ml each), 100 mg of the produced $MgTiO_3$ powder was suspended. The necessary quantity of metal salt AgNO3 (0.01M; 928-4636µL) corresponding to the required weight percentage (1 wt%) was added to these suspensions. Test tubes were securely sealed with a rubber septum following a 20-minute argon (Ar) gas purge to produce an inert atmosphere. The test tube contents were continuously stirred by magnetic means in a photochemical reactor for three hours while being revealed to UV illumination (125 W, 10.3 mW/cm^2). The metal-deposited solutions were then subjected to centrifugation at 8500 revolutions per minute, Frequently cleaned with ethanol and deionized water, followed by drying for two hours at 70 °C in an oven. The obtained Ag-deposited nanocomposites have the following names: 1, 2, and 3 weight percent Ag-$MgTiO_3$.

2.5. Characterization techniques

The produced samples were subjected to crystallographic examinations using an X-ray powder diffraction Panalytical-Xpert-PRO machine that was outfitted with a Cu-Kα radiation source (1.54 Å) that operated at 45 kV and a diffraction angle (2θ) that ranged from 10° to 80° at a 5°/min scan rate. Using a spectrofluorometer (Perkin-Elmer LS55), the photoluminescence (PL) emission spectrum was measured to investigate the separation of photogenerated electron-hole pairs. Both high-resolution transmission electron microscopy (HRTEM TALOS F200S G2 model running at 200 kV voltage) and scanning electron microscopy (SEM; JEOL JSM-7600F operated at 30 kV) were

used to analyze the materials' size and shape. The elemental composition ratio was analyzed using energy-dispersive spectroscopy (SEM-EDS, JEOL JSM-7600 F) at 30 kV.

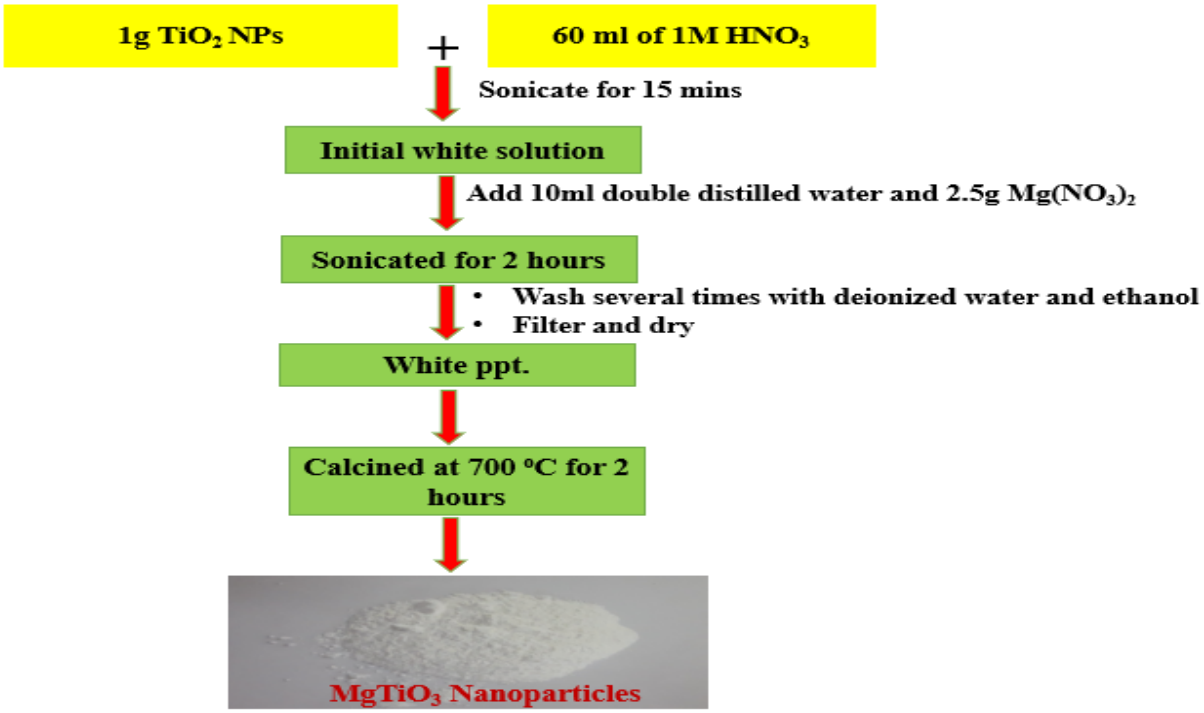

Scheme-1. Flow chart of synthesis of $MgTiO_3$ nanoparticles

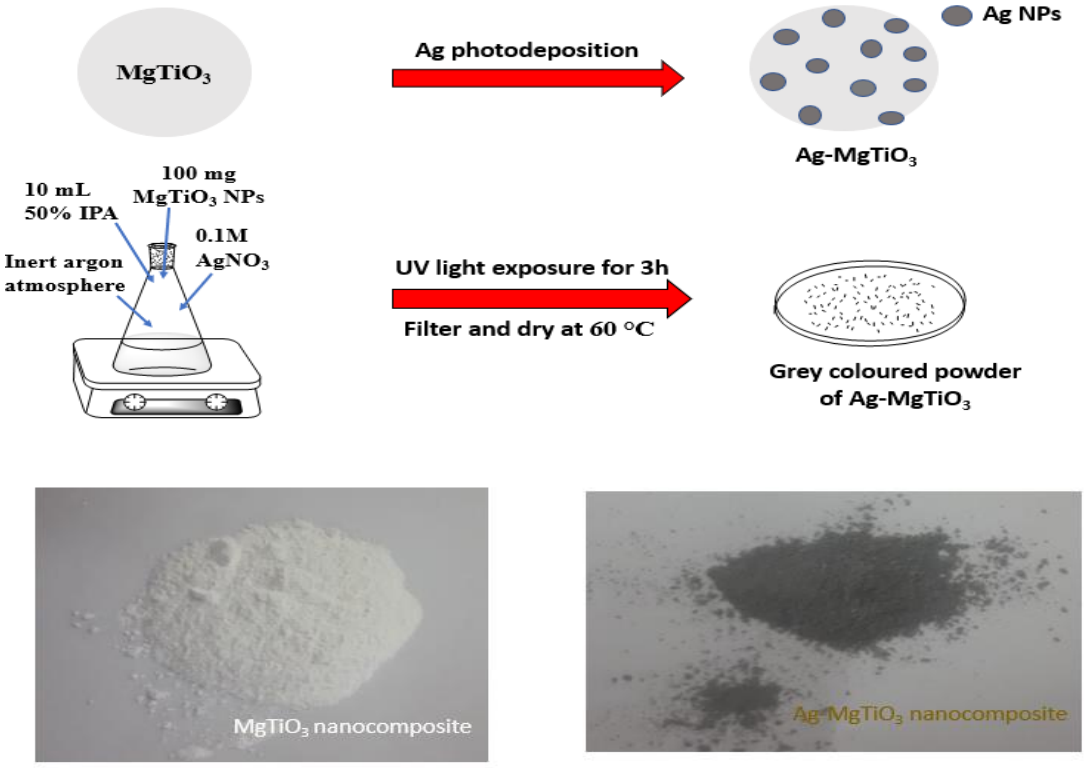

Scheme 2: Experimental procedure for photo-deposition of Ag nanoparticles onto $MgTiO_3$.

The catalyst's oxidation status was investigated using X-ray photoelectron spectroscopy (XPS, KRATOS axis 165 Shimadzu) with Mg-Kα radiations at 75 W. The optical absorption properties of powder solid samples were explored using an Avantes DRS instrument and a UV-vis spectrophotometer (JASCO, V-750), over a spectral range of 200-800 nm, with BaSO4 as a reference standard.

2.6. Photocatalytic degradation of organic waste

The photocatalytic efficiency of the produced materials ($MgTiO_3$ and silver-modified $MgTiO_3$) was tested using Fuchsin (Fuc) dye Deterioration. The photocatalytic process was carried out under direct sunlight. 3 mg of photocatalyst was dispersed into 10 mL of Fuc solution (10 ppm) at a 0.3 g/L concentration. Before irradiation, the suspensions were agitated in the absence of light for 40 minutes to establish an Equilibrium of adsorption and desorption processes between the dye molecules and the catalyst's surface. To initiate deterioration, the solution was stirred for 110 minutes with the vessel horizontal and exposed to direct sunlight. After removing the $MgTiO_3$ catalyst, roughly 5–6 mL of the solution was taken out and examined with a UV-visible spectrophotometer at intervals. The photocatalysis studies occurred at the Thapar University in Patiala, India, in a subtropical region. The study spanned from April 17 to May 15, 2024. Using a LICOR pyranometer, the median sunlight exposure intensity was determined to be 845 W/m^2. The solution was exposed to visible illumination from a 45 W CFL lamp (Philips) at a brightness of approximately 100 W/m^2.UV light was applied to the solution using a 100 W Hg lamp at 365 nm with a flux density of 64–66 W/m2. Each experiment was performed four times, and graphical representations were created with error margins representing a 4% data source error. The absorbance spectrum of Fuc was measured at frequent intervals, specifically at λ_{max} = 547 nm. The photodegradation efficiency was computed using the formula below:

$$\text{Deterioration effictiveness } (\%) = \{(C_0 - C_t)/C_o\} \times 100 \quad (1)$$

Here, C_0 denotes the initial concentration of Fuc prior to light exposure at time '0', and C_t is the concentration of Fuc following light exposure at the time 't.'

3: RESULTS AND DISCUSSION

3.1 Surface structural studies:

XRD (X-ray diffraction) evaluation: XRD analysis was employed to forecast the prepared samples' crystal structure and phase composition. Figure 1 depicts the XRD profiles of $MgTiO_3$ and Silver-

deposited $MgTiO_3$ samples at optimal 1 wt%. The $MgTiO_3$ structure has twelve main reflection peaks at the diffraction angle (2θ) readings of 19.25°, 21.28°, 24.03°, 32.79°, 35.53°, 40.64°, 49.135°, 57.10°, 62.08°, 63.78°, 71.22°, and 75.28°. These correspond to the (003), (101), (012), (104), (110), (113), (024), (116), (018), (214), (300), and (220) crystal planes, respectively (Reference pattern 01–079-0831) [28]. In addition to the diffraction peaks, the minor secondary phase TiO2 peak at (2θ) 27.38 is indicated by "♣" asterisks on the graph. The XRD pattern of Ag-$MgTiO_3$ has two low-intensity peaks at 2θ values of 38.2˚ and 44.1, which relate to the (111) and (200) planes of metallic Ag, respectively. These peaks are denoted with **"⁎"** asterisks in the graph. The fact that the silver Nanoparticles are well-loaded or disseminated on the surface instead of being embedded into the $MgTiO_3$ lattice is further supported by the fact that the $MgTiO_3$ peak location did not alter.

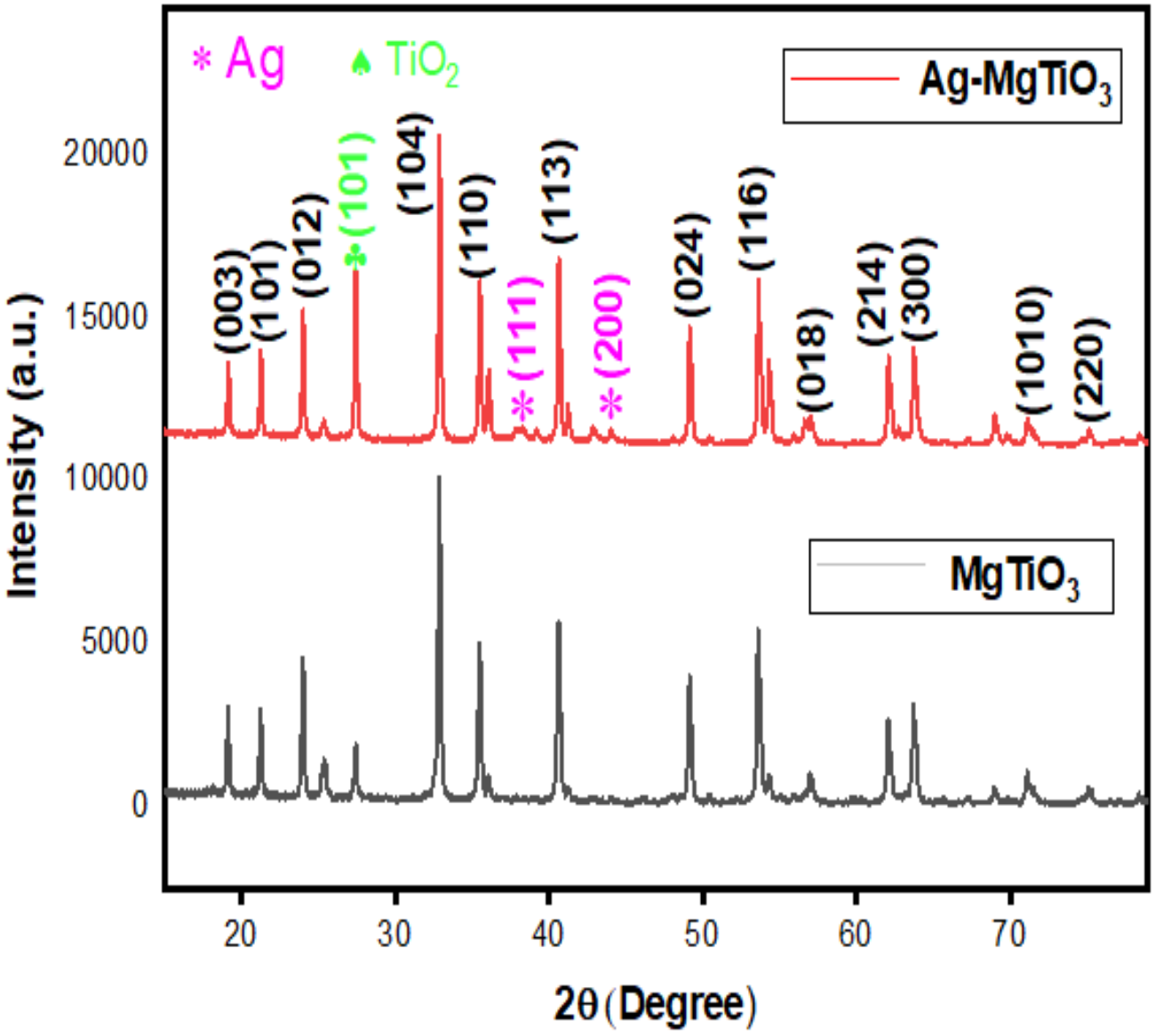

Fig. 1: X-ray diffraction profiles of $MgTiO_3$ and Ag-$MgTiO_3$ nanocomposites.

3.2 Morphological study:

The surface pattern of the catalysts was characterized by employing Fe-SEM and HR-TEM analyses. Fig. 2(a)–(b) shows FE-SEM images of $MgTiO_3$ and optimal 1wt% Ag-$MgTiO_3$ composites. All samples showed predominantly spherical clumps or clusters. The formation of clumps may be caused by a high calcination temperature of 700 °C. FE-SEM was unable to distinguish between the deposited silver nanoparticles and pure MgTiO3 due to the low weight % of Ag deposited. However, the elemental composition data supports their presence on the $MgTiO_3$ surface. EDS analysis was utilized to determine the amount of elements found in the composite materials. Figures 2 (a)–(b) show separate EDS spectra and tables revealing elemental content data. The anticipated loading amount of Ag was 1wt%, whereas the observed value was 0.29%. The reduced Ag concentration could be attributed to selected area selection for EDX, mass loss during photo deposition, or washing.

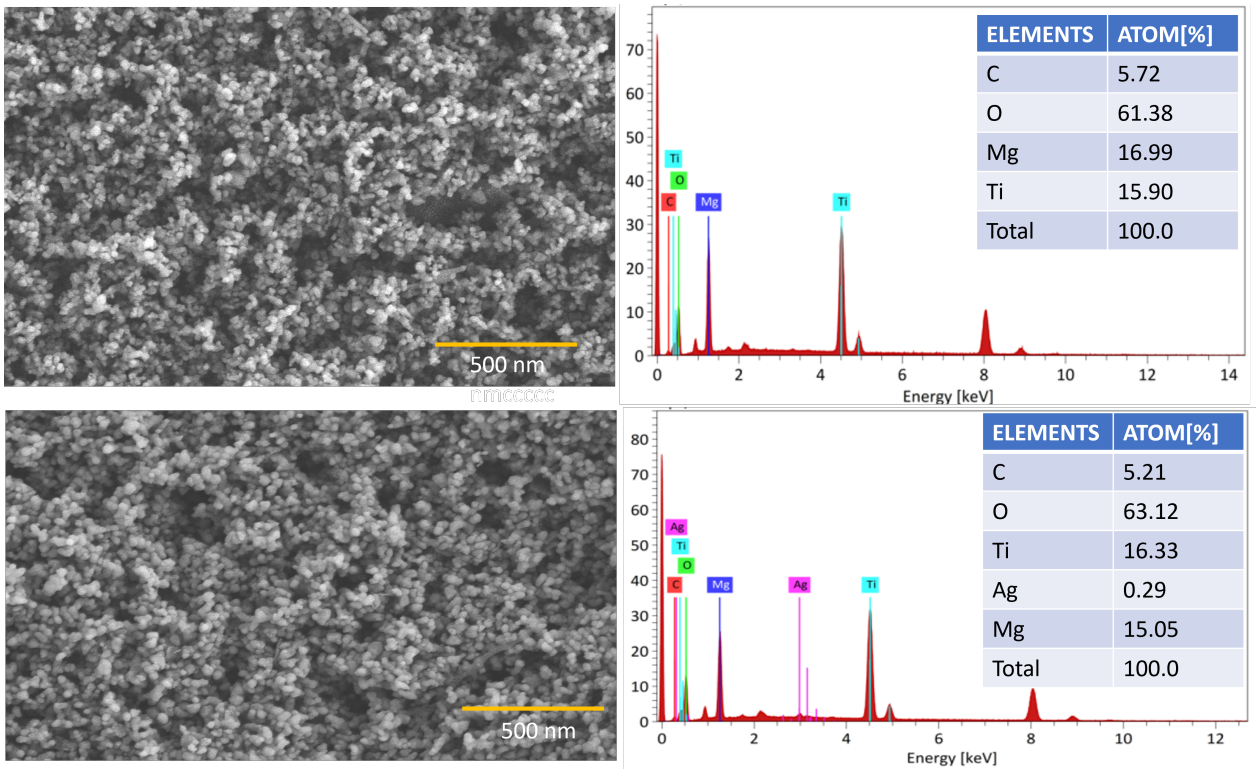

Fig.2: Field Emission Scanning Electron Microscopy images of (a) $MgTiO_3$, (b) 1 wt% silver-modified $MgTiO_3$ and their corresponding EDX profiles.

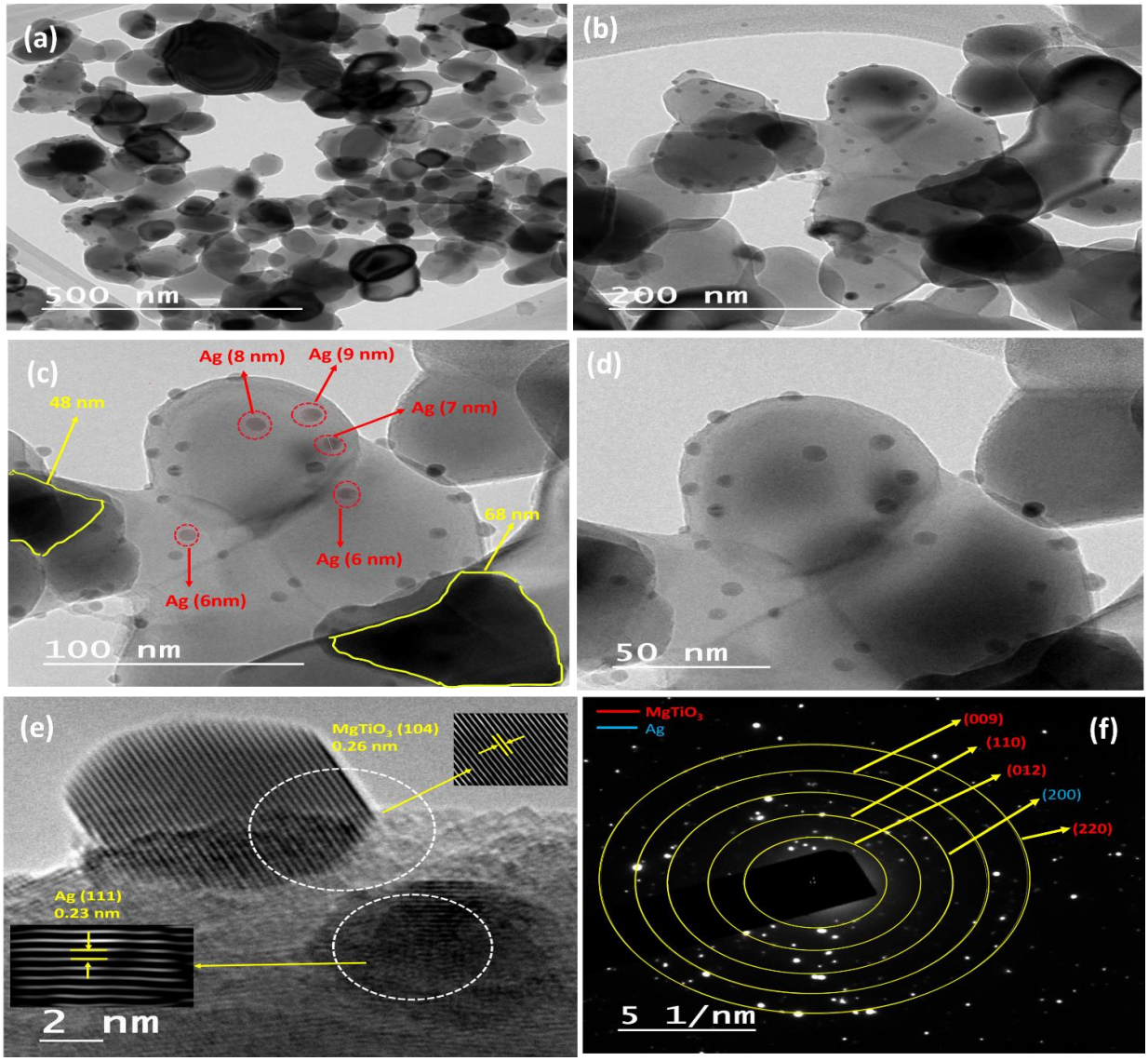

Fig. 3: High-resolution TEM micrographs of (a-d) Ag-$MgTiO_3$ photocatalyst (e) associated lattice fringes and (f) SAED pattern for Ag-$MgTiO_3$ composite.

3.3. Oxidation state analysis by XPS

XPS was used to analyze each element's valence states and chemical composition in the Ag-$MgTiO_3$ nanocomposite. The outcomes are depicted in **Figure 4.** The survey spectrum shows clear peaks for Mg, Ti, O, and Ag (Fig. 4(e)). The detailed XPS spectra of Mg (1s) (Fig. 4(a)) centered at 1304.6 eV match up with the Mg^{2+}. Figure 4(b) shows two distinct binding energy peaks at 458.7 eV and 464.5 eV, inferring that the oxidation state of Ti is +4. Fig. 4(c) depicts the deconvoluted spectra of O 1s, segmented into two separate peaks.

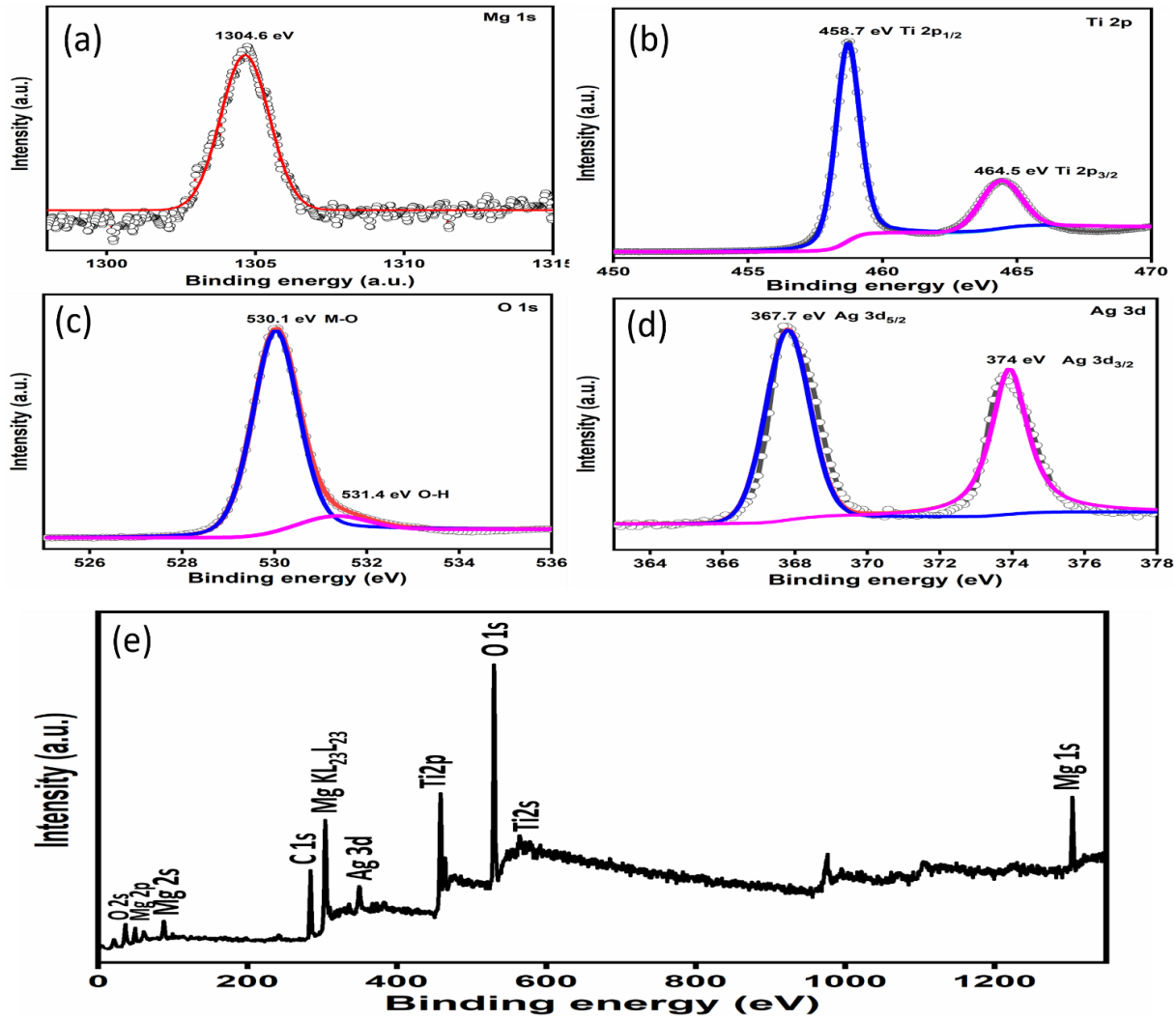

Fig. 4: XPS spectra of Ag-$MgTiO_3$ nanocomposite (a) Mg 1s, (b) Ti 2p, (c) O 1s, (d) Ag 3d, (e) survey scan.

One at a (Binding Energy) of 530.01 eV is assigned to oxygen in the $MgTiO_3$ crystal lattice, and the latter peak at 531.4 eV is attributed to the oxygen atom of O-H group bound to the surface of $MgTiO_3$ in the nanocomposite. The spectra of silver 3d (Fig. 4(d)) contain two distinct peaks, Ag $3d_{5/2}$ (367.7 eV) and Ag $3d_{3/2}$ (374.0 eV).

3.4 Porosity and Surface Area Evaluation

The BET-specific surface area graph of the Ag-$MgTiO_3$ nanocomposite and bare $MgTiO_3$ nanocomposite is depicted in Fig. 5. The nitrogen adsorption and desorption isotherms of both samples, classified by the IUPAC, exhibited type-IV Langmuir isotherm profiles with characteristic H_3-structured hysteresis loops, suggesting their multi-layered design and mesoporous nature. Both samples' major pore sizes are between 3 and 21 nm, which supports the idea that the catalysts are made of mesoporous material. The Ag-$MgTiO_3$ composite (16.67 m2/g) has a lower BET-specific

surface area than pristine MgTiO3 (20.247 m2/g). This modest drop in surface area could be attributed to Ag NPs populating the pores of mesoporous $MgTiO_3$. Despite a minor decrease in surface area, this may not have diminished photocatalytic efficiency, which is also reliant on other parameters such as material band gap, electron transport between plasmonic Ag and $MgTiO_3$, and suppression of electron-h^+ recombination, as Table illustrates in Fig. 5. Furthermore, the pore volume and size range of the Ag-$MgTiO_3$ nanocomposite was found to be slightly increased. Loading metallic silver nanoparticles into the $MgTiO_3$ surface may be responsible for the expansion in the different BET parameters. This would provide many active zones for contaminant adsorption and speed up the movement of reactants and products, both of which are necessary to achieve high photocatalytic activity.

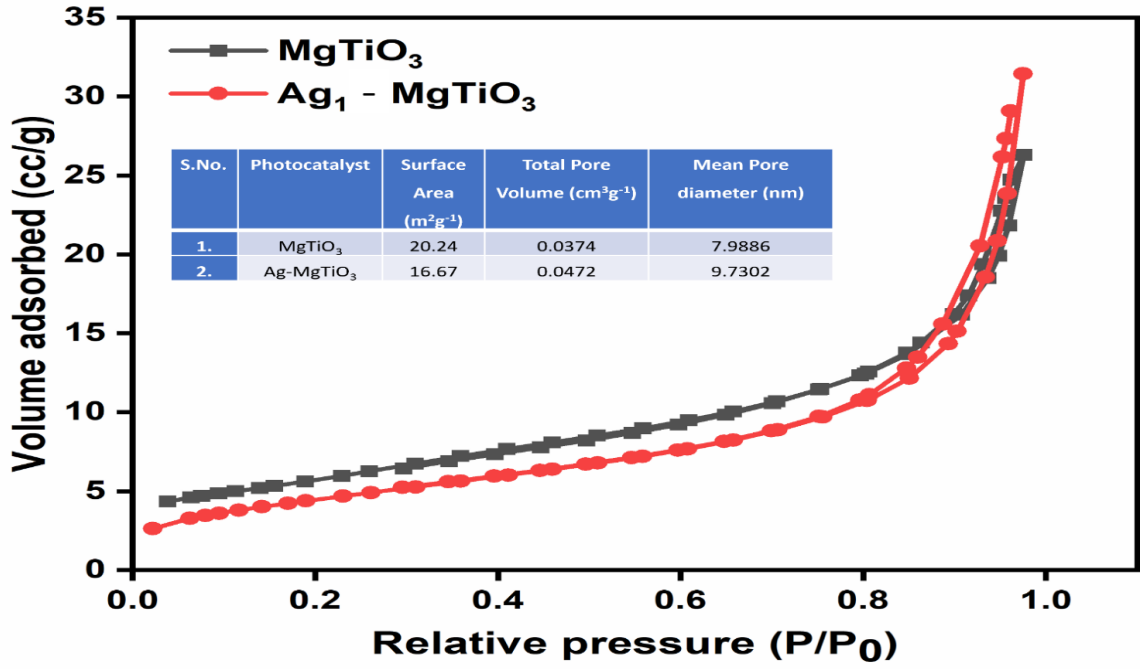

Fig. 5: Nitrogen adsorption isotherms curves of $MgTiO_3$ and Ag-$MgTiO_3$ nanocomposite.

3.5 Vibration mode analysis by RAMAN spectra

Figure 6. displays the Raman spectrum comparison of the Ag-$MgTiO_3$ and $MgTiO_3$ samples. The Raman spectrum of pure magnesium titanate ($MgTiO_3$) has multiple characteristic peaks at 225, 271, 291, 318, 351, 397,432,483, 632, and 716 cm^{-1}, which correspond to Ag, Eg, Ag, Eg, Eg, Ag, Eg, Ag, Eg, and Ag symmetry. Additional peaks at 162 cm^{-1} may be due to unreacted starting precursors[30,31]. The peak at 225 cm^{-1} is primarily due to vibrations between Mg and O atoms. The broad, strong signals at 318 and 352 cm^{-1} are due to the O-Ti-O bending vibration within the TiO_6 group of $MgTiO_3$. The higher frequency peak at 716 cm^{-1} indicates symmetric Ti-O stretching

vibrations. After Ag-decoration, all modes showed a slight peak broadening, which might be attributed to scattering contributions outside the Brillouin zone [32]. The Eg peak at 318 and 351 cm^{-1} shows a significant drop in intensity, demonstrating the fall in crystallinity of $MgTiO_3$ nanostructures with Ag loading [33].

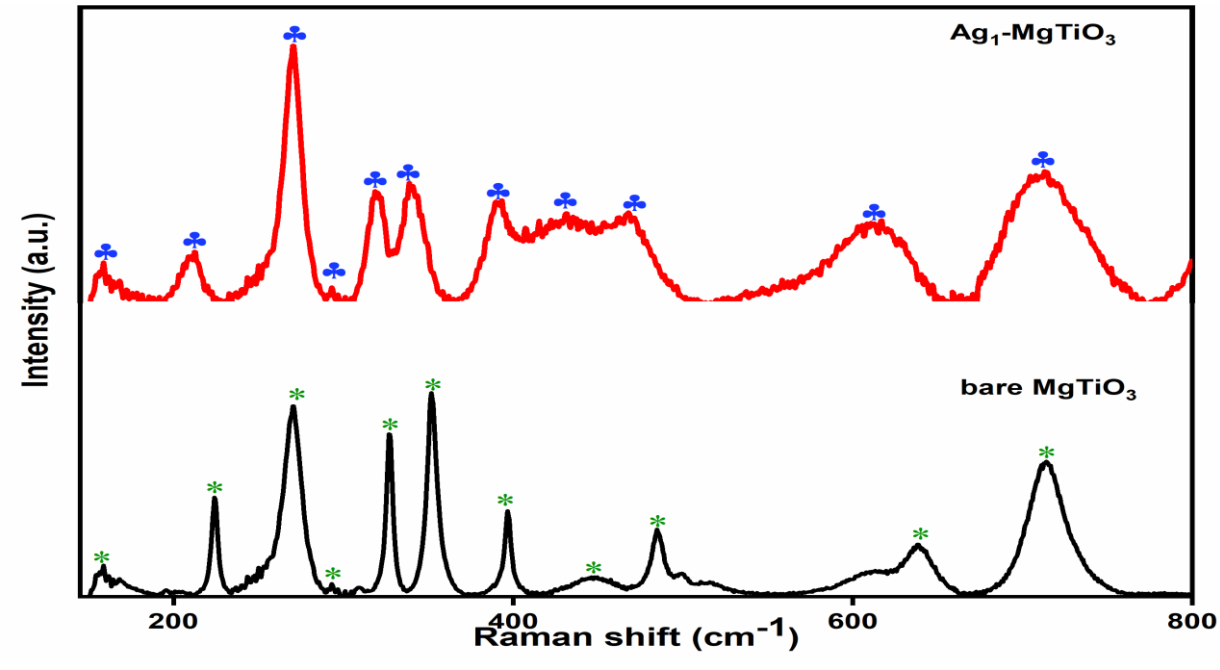

Fig 6. Raman spectra of $MgTiO_3$ and the Ag-$MgTiO_3$ nanocomposite.

3.6. Optical and charge transfer specifications

UV-Vis Diffuse reflection measurements

Figure 7. Depicts the U-V spectra of bare and 1 wt% Ag-$MgTiO_3$ composites. $MgTiO_3$ exhibited a peak in the UV region, possibly indicating a transition of electrons from the valence to the conduction band. After the deposition of silver, the composite range of absorption moved dramatically toward visible light. LSPR bands for silver in composites were observed at 506 nm. Ag-$MgTiO_3$ composites exhibit UV and visible absorbance maxima, indicating their high photoactivity and ability to respond in the full-range spectrum.Depositing Ag metal on the $MgTiO_3$ surface resulted in a color change from white ($MgTiO_3$) to grey (Ag-$MgTiO_3$) (see Scheme 2). This demonstrates that the deposited metal alters the light absorption capabilities of $MgTiO_3$. Additionally, the band gap energies of the samples were determinate through the Tauc relation, given by: $\alpha h\nu = A\ (h\nu - Eg)^n$ where α = absorption coefficient, $h\nu$ = photon energy, A = constant, Eg = the band gap of the material and n is the exponent coefficient (n=2 for direct band gap). The exact band gap value was computed by plotting the graph between $(\alpha h\nu)^2$ versus $h\nu$. The Eg values of the $MgTiO_3$ and Ag-$MgTiO_3$ samples were designed to be 2.95 eV and 2.75 eV.

The band gap value decreases notably from 2.95 to 2.75 eV upon the deposition of silver onto $MgTiO_3$. The Ag-$MgTiO_3$ catalyst has a narrower band gap than the $MgTiO_3$ catalyst. Based on DRS spectra findings, it could be concluded that enhancing the visible-illumination absorption effectiveness here would favor the generation of numerous charge carriers and thus elevate the photocatalytic efficiency of the metal-loaded composite.

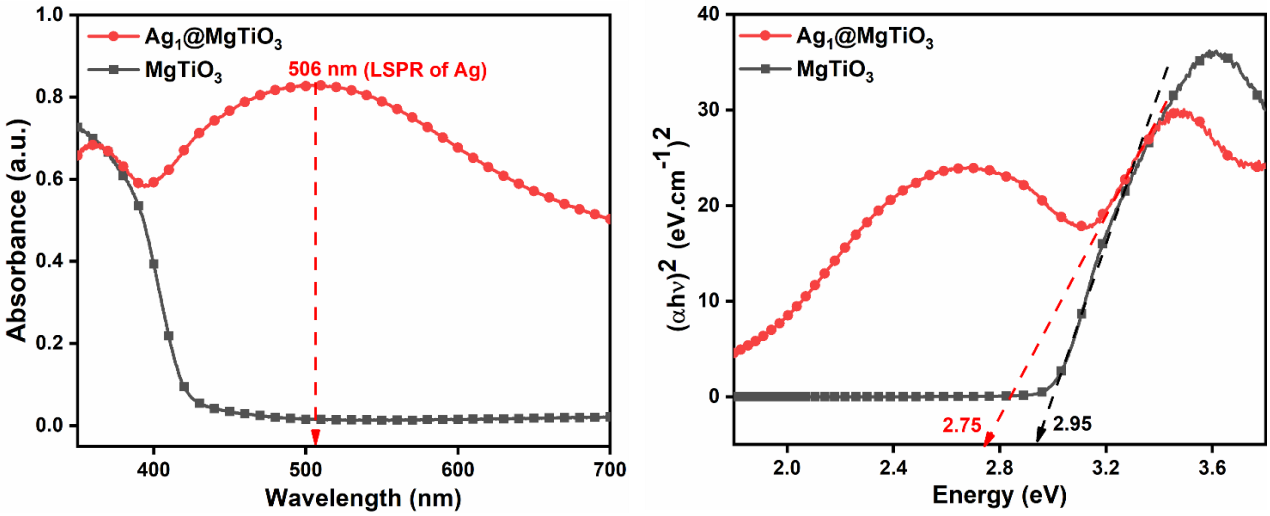

Figure 7. UV-Vis diffuse reflectance spectra and (b) a graph of $(\alpha h\upsilon)^2$ against $h\upsilon$ (eV) to determine the band gap of $MgTiO_3$ and Ag-$MgTiO_3$ nano-sized particles.

Photoluminescence studies

PL spectroscopy was employed to evaluate the separation of charge carrier efficiency across several samples. PL strength is generally recognized as directly related to the rate of electron-hole pair recombination: higher recombination rates result in stronger PL signals, whereas lower rates result in weaker signals [34]. Figure 8. depicts the PL spectra recorded at room temperature for both $MgTiO_3$ and Ag-$MgTiO_3$ nanocomposites excited at 335 nm. Both samples show peaks at 423, 486, and 530 nm. The 423 nm peak relate to near-band edge emission, whereas the 486 and 530 nm peaks correspond to deep-level emissions. The near-band edge peak in the UV range is caused by the reformation of charge carriers generated by stimulation with energy equal to or surpassing the bandgap. DLE peaks in the visible area are associated with inherent defects such as oxygen vacancies (VO), titanium vacancies (VTi), and imperfections on the surface. The addition of Ag did not significantly affect the band edge positions, but it did cause a considerable decrease in PL intensity when compared to bare $MgTiO_3$. This reduction indicates a decrease in the reformation rate of photoinduced electron-hole pairs in the silver-modified $MgTiO_3$ composites. This effect is most likely owing to Ag's capability to trap electrons, which improves charge transfer from the $MgTiO_3$ surface

to the silver particles, minimizing reformation and increasing the lifetime of charge carriers. The highest PL quenching occurs in 1 wt% Ag-$MgTiO_3$ nanocomposites, indicating that this Ag concentration is ideal for effective electron transport. Enhancing the silver content beyond 1 wt% leads to an increase in PL intensity, likely due to overwhelming metal loading that covers the $MgTiO_3$ surface. This excess metal can increase the rate of electron-hole reformation and decrease photocatalytic effectiveness. Among the two samples, the 1 wt% Ag-loaded $MgTiO_3$ had the lowest PL signal.

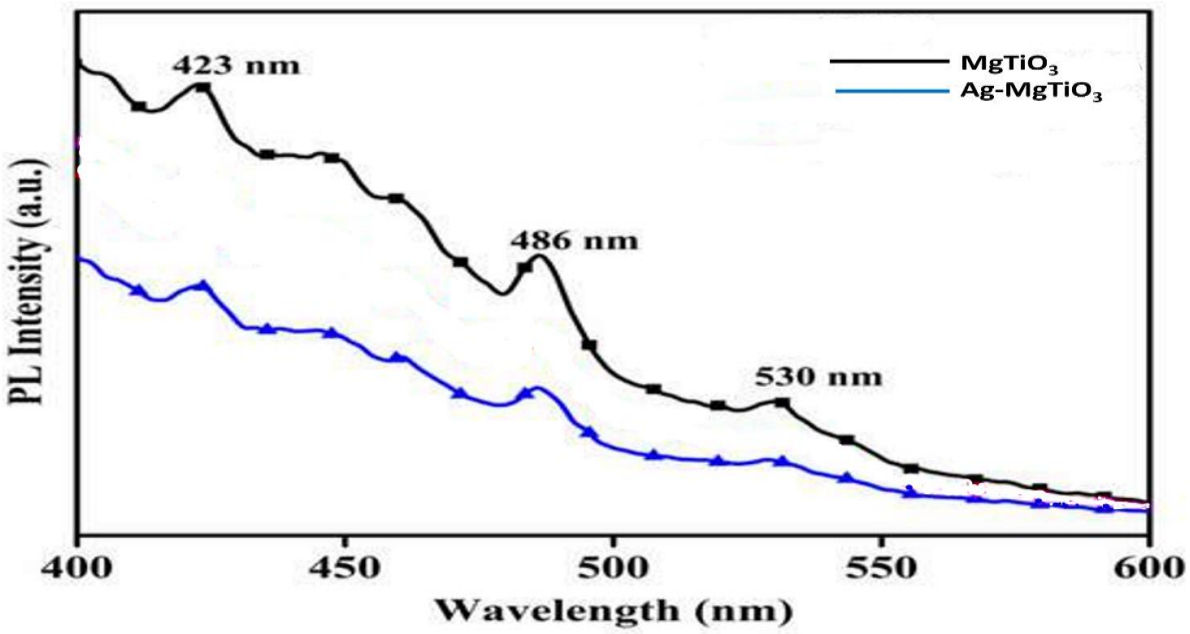

Fig. 8: Photoluminescence (λ_{max} = 335 nm) spectra of bare $MgTiO_3$ and Ag- $MgTiO_3$ nanocomposites.

3.7. Photocatalytic activity

3.7.1. Photocatalytic degradation

The light-driven catalytic efficiency of the Ag-$MgTiO_3$ nanocomposite was initially assessed by investigating the UV light, Visible light, and sunlight-induced breakdown of the cationic dye fuschin blue (Fuc) (Fig. 9 (a-b)).To provide a comparison, Fuc was removed from the bare $MgTiO_3$ and Ag-$MgTiO_3$ composites. Along with photocatalysis, assessments on photolysis and adsorption were carried out, and the findings are shown in Figure 9(a). In the nonexistence of a photocatalyst, just 12% of Fuc is destroyed after 50 minutes of direct sunlight exposure, suggesting its remarkable steadiness.

Following 30 minutes of dark adsorption, the adsorption effectiveness of several composites was computed: $MgTiO_3$: 13.16%; Ag-$MgTiO_3$: 18.21%. Ag-$MgTiO_3$ exhibits higher adsorption towards Fuc than unmodified $MgTiO_3$, and when Ag is integrated onto the surface of $MgTiO_3$, its adsorption capacity increases, which is attributed to the increased BJH pore volume, size, and adsorption sites. Furthermore, natural sunlight was irradiated before the photocatalytic process to improve removal efficiency. After 50 minutes of light exposure, the nanocomposites advance according to the outlined progression: Ag-$MgTiO_3$ (99.2%) > $MgTiO_3$ (55.6%) {Fig. 9(c-d)}. Thus, the Ag-$MgTiO_3$ exhibits dynamic Fuc elimination, which is consistent with previous characterization findings. Furthermore, utilizing pseudo-first-order rate kinetics, the related reaction rate constants (k) were Determined through numerical analysis,

$$\{\ln(C_t/C_0) = -kt\} \quad (2)$$

Here C_0 is the initial concentration of C_V, C_t is its concentration at the time (t), and k denotes the rate constant (min^{-1}). Figure. 9(f) compares the $\ln(C_t/C_0)$ readings for the various samples based on the extent of their exposure to light. The Ag-$MgTiO_3$ photocatalyst had a high Fuc degrading rate constant (0.04591 min^{-1}), which is nearly 3.336 times greater than that of pristine $MgTiO_3$ NRs. It is apparent that the intensity of the maximum absorption peak of the characteristic feature increases as illumination time lengthens during deterioration, Fuc dye at 546 nm is observed to diminish progressively by both catalysts. The Ag-$MgTiO_3$ nanocomposite showed a markedly greater decline after 50 minutes of sunlight irradiation. The comprehensive reducing pattern seen in the Fuc spectral analysis demonstrates the superior photocatalytic efficiency of Ag-$MgTiO_3$ suggesting that the Ag loading helps enhance the photocatalytic activity of $MgTiO_3$. The experimental results show that adding Ag on the surface of $MgTiO_3$ considerably improves its degrading performance. These metallic coatings operate as electron accumulation sites, catching photo-excited electrons from the $MgTiO_3$ surface and transferring them to oxygen molecules. This process enhances the production of highly reactive electrons and superoxide radical anions ($\cdot O_2^-$), which are essential for successfully decomposing Fuc. To get deeper insights into the improved photoactivity of $MgTiO_3$, the valence band and conductance band potentials of $MgTiO_3$ relative to the Normal Hydrogen Electrode were calculated based on its band gap using Equations. **(3)-(4):**

$$E_{CB} = X - E_e - 0.5Eg \quad \textbf{(3)}$$

$$E_{VB} = X - E_e + 0.5Eg \quad \textbf{(4)}$$

In this equation, X represents the absolute electronegativity of $MgTiO_3$ (5.12 eV), Ee is the energy of free electrons on the hydrogen scale (4.5 eV), and Eg is MgTiO3's band gap (2.75 eV). The computed Conduction and Valence potentials were found to be -0.755 V and 1.995 V vs NHE.

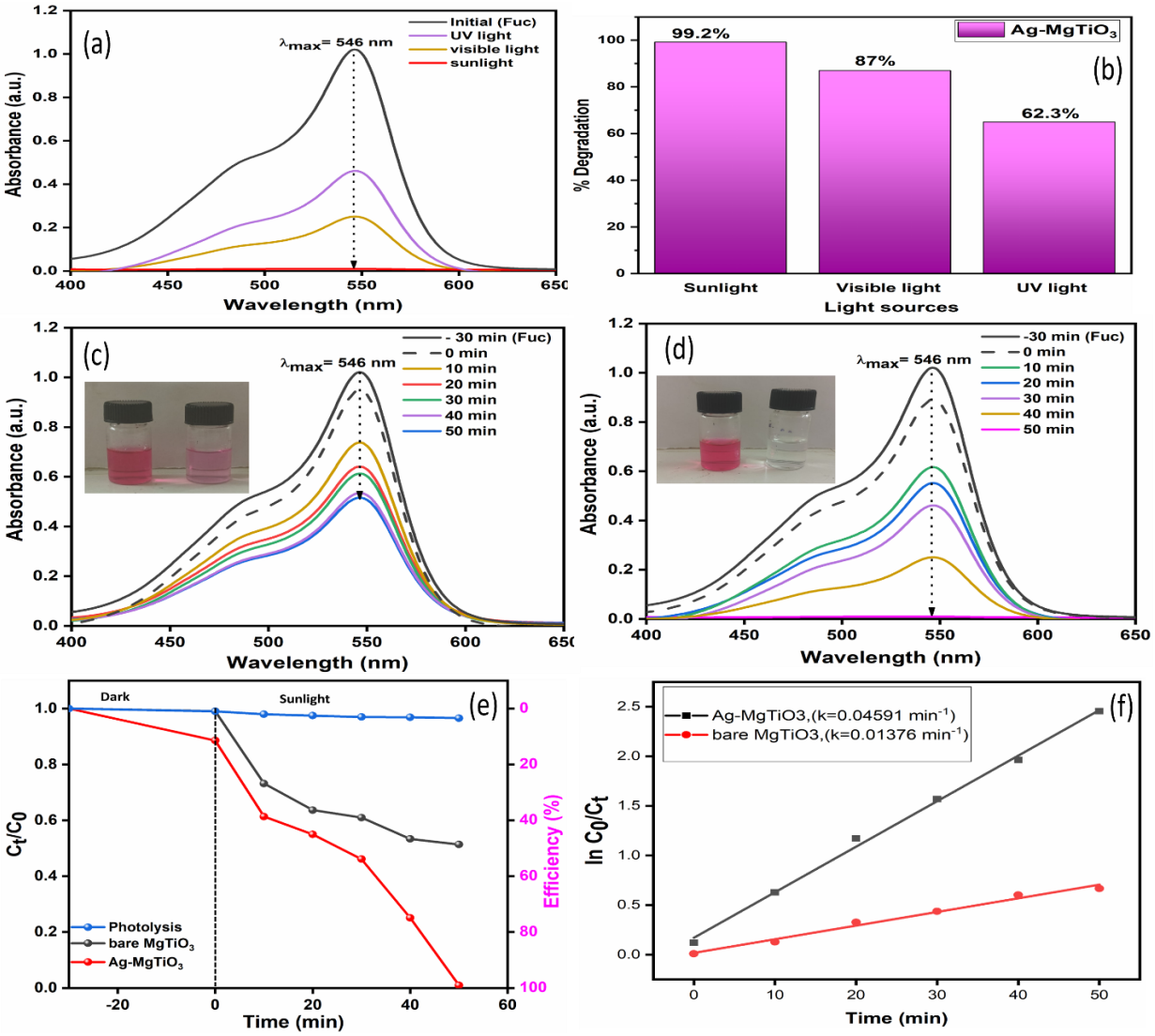

Fig. 9: (a-b) Shows degradation efficiency of Fuchsin dye using Ag-$MgTiO_3$ photocatalyst in various light sources, (c-d) demonstrates the variations in the UV-vis absorption spectrum of the Fuchsin dye solution over both catalysts ($MgTiO_3$ and the Ag-$MgTiO_3$ sample) across different exposure durations, (e) Kinetic plots over time and (f) the associated variations in apparent reaction rate constants (k) for the deterioration of Fuchsin dye under the influence of distinct photocatalysts.

3.7.2 Effect of visible/sunlight illumination: Under ideal conditions, relative studies assessed photocatalytic activity utilizing various light sources, including UV, visible, and natural sunlight. As shown in Fig. 9(a-b), pollutants deteriorated at an efficiency of 62.3% under UV irradiation and 87% under visible irradiation. Notably, using the Ag-$MgTiO_3$ nanocomposite under natural sunlight resulted in the best removal efficiency of 99.2%. These findings highlight the superior

effectiveness of natural sunlight in pollutant degradation in conjunction with the proposed photocatalyst. Thus, natural sunlight has a significant advantage over non-natural light sources for Contaminant breakdown.

3.7.3 Influence of amount of catalyst: The correct amount of catalyst utilized considerably impacts the photocatalytic process' efficiency. Using the appropriate catalyst quantity is critical to avoid overuse, Potentially causing particle clustering. Furthermore, utilizing the appropriate amount ensures maximum photon absorption, which improves photodecomposition efficiency. Experiments Were performed to determine the impact of catalyst concentrations ranging from 0.1 to 0.5 g/L on dye photocatalytic degradation. It was observed that raising the photocatalyst dose from 0.1 to 0.3 g/L significantly improved degradation efficiency, reaching around 99.2% at 0.3 g/L. This increase is due to the increased number of active reaction sites caused by the larger catalyst quantity. However, as the concentration increased to 0.4 g/L, degradation efficiency dropped. This drop can be due to the solution becoming opaque, resulting in light dispersion and decreased effectiveness in the solution. Furthermore, at greater concentrations, the dye fully coats the catalyst surface due to full adsorption, making further catalyst embedding useless. This saturation causes the deactivation of active sites, reducing their efficiency. Consequently, the optimal concentration for future studies was 0.3 g/L of photocatalyst[35].

3.8 Mineralization of dye by TOC measurement

As mineralization is the end goal of pollutant treatment, Total Organic Carbon (TOC) testing was employed to determine how effectively contaminant molecules were mineralized during photocatalysis. The TOC value generally represents the quantity of organic carbon dissolved in the aqueous solution, and a decline in the concentration of TOC provides insight into the level of mineralization of the organic substance upon completion of the reaction. TOC was analyzed at the beginning and end of the photodegradation process to determine the amount of Fuc dye mineralization over the fabricated Ag-MgTiO3 photocatalyst. The TOC removal efficiency of the Ag-$MgTiO_3$ photocatalyst for removing Fuc dye was examined using a dichromate-based chemical approach. The findings demonstrate that the TOC values of Fuc dye decreased from 27.7 to 8.9 mg/l after 50 minutes of direct sunlight exposure, representing a 67.8% TOC reduction. The decreased TOC values indicate that the Ag-$MgTiO_3$ photocatalyst will mineralize Fuc pollutants. Furthermore, degradation efficiencies obtained from the UV-Vis spectrophotometer were higher than the mineralization activity. The slow rate of both photodegradation and mineralization is evident from the partial mineralization of pollutants. This is primarily due to the creation of intermediate products as studied

by HRMS studies. Complete mineralization of the remaining intermediates is possible, but it will likely need additional sunlight exposure.

3.9 Scavenger studies

Radical capture studies were carried out to understand better how active species in Ag-$MgTiO_3$ nanocomposite engaged in photocatalytic removal of Fuc as well as propose a mechanism. Various scavengers ($K_2Cr_2O_7$, benzoquinone, IPA, and methanol) Were assigned as quenchers of e^-, $O_2^{\bullet-}$, $^{\bullet}OH$, and h^+ radicals. As shown in Fig. 10, Under identical conditions as degradation experiments, revealed that the photo removal effectiveness of Fuc was decreased in the presence of quenchers listed according to their significance in the following sequence Methanol > IPA > $K_2Cr_2O_7$ > Benzoquinone, indicating that $O_2^{\bullet-}$ and e^- radicals are the primary contributors, with •OH playing a minor role. These results demonstrate that e^- and $O_2^{\bullet-}$ are important reactive species in Fuc photocatalytic degradation.

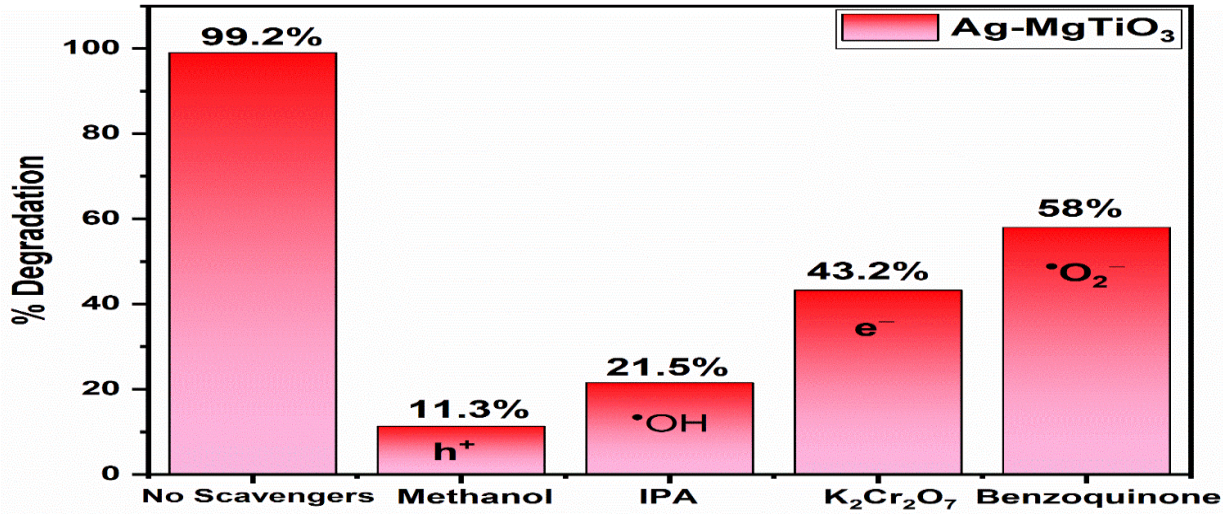

Fig 10: Impact of a set of scavengers on Fuchsin dye degradation by Ag-MgTiO3 nanocomposite.

3.10 Photocatalytic degradation pathways

Based on the HRMS data, two degradation routes of fuchsin dye are suggested and provided in Fig. 12. Several fragments of smaller molecular masses than fuchsin dye are observed in the HRMS chromatogram, out of which the structures of compounds with peaks at m/z = 316, 302, 223 have been identified. In pathway 1, the fuchsin dye (m/z = 365) undergoes the loss of a methyl (-CH_3) group to give the fragment with m/z = 316, which further loses a -CH_3 group, forming the fragment with m/z = 302. In pathway 2, the fuchsin dye can undergo the loss of a 2-methylaniline ring, thus

forming the intermediate with m/z = 223. Further, prolonged solar or UV/visible irradiation may be required for these fragments of fuchsin dye to fully mineralize into CO_2, H_2O, and other simple molecules compared to what has been investigated here [36].

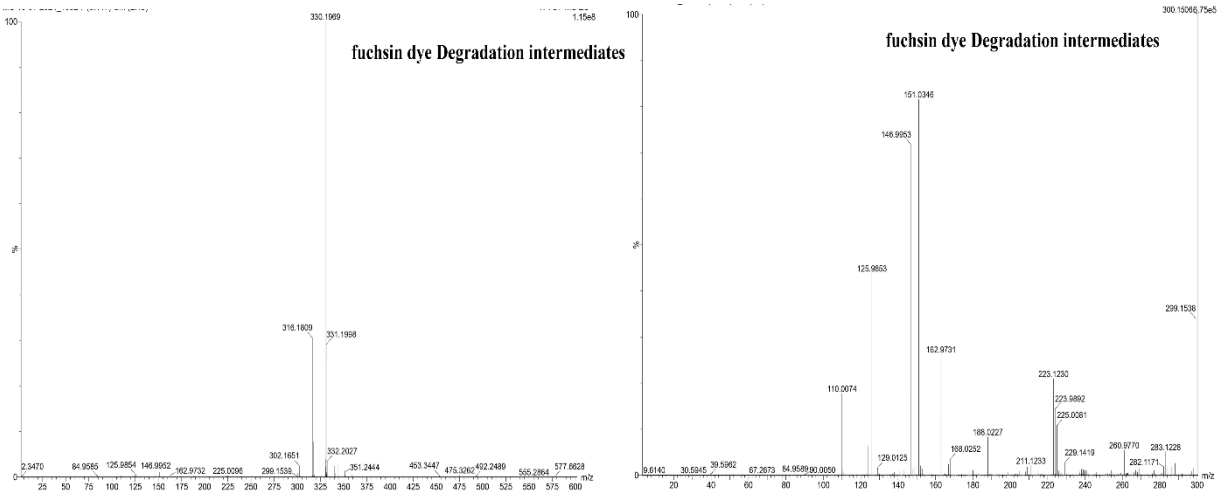

Fig 11. The mass spectra of Fuchsin dye after photodegradation using Ag-$MgTiO_3$ catalyst

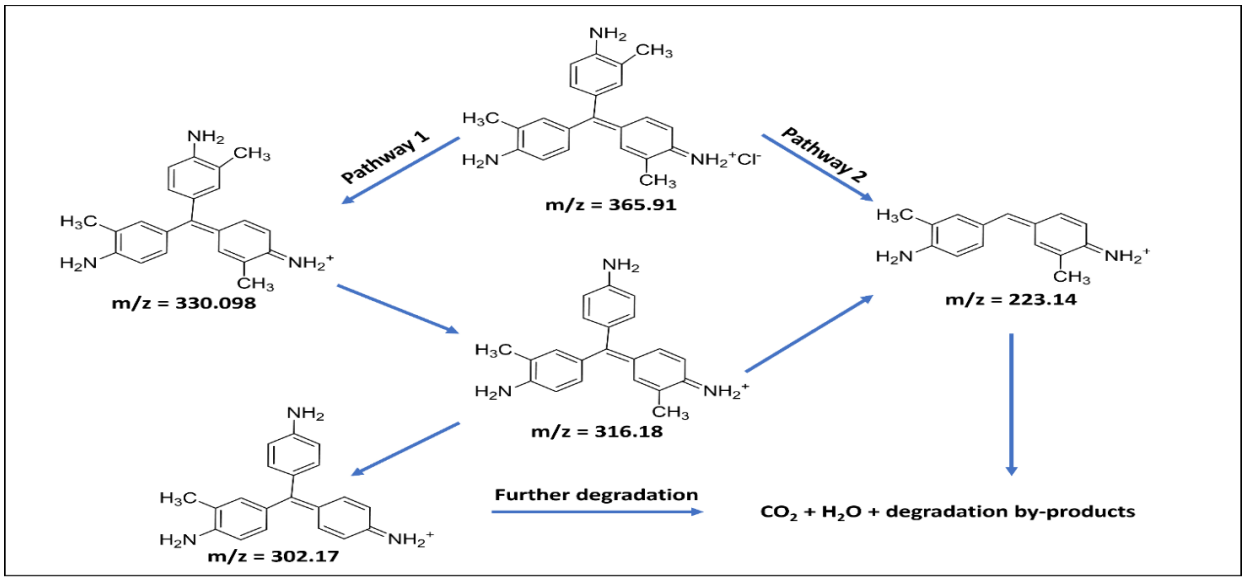

Fig 12: Degradation pathway of Fuchsin dye using Ag-$MgTiO_3$ photocatalyst under sunlight.

3.11 Possible degradation mechanism

Scheme 3. depicts the mechanism responsible for the degradation of Fuc under sunlight using the as-prepared catalysts. When exposed to light, electrons in $MgTiO_3$ are excited from the valence band to the conduction band, forming holes (h^+) in the Valence Band. These photoexcited electrons and holes subsequently interact with adsorbed oxygen and water molecules, resulting in reactive oxygen species including superoxide radical anions ($\cdot O_2^-$) and hydroxyl radicals ($\cdot OH$). These highly oxidative species work together to effectively degrade or mineralize Fuc. In contrast, Ag has a lower redox

potential (+0.799 V vs. NHE) than $MgTiO_3$'s CB potential (-0.75 V), which allows photoexcited electrons to flow quickly from MgTiO3 to the Ag surface. This speeds up the separation of electron-hole pairs within $MgTiO_3$. The deposited Ag functions as an electron sink or trap, preventing the electron-hole reformation process. The overall reactions during photocatalysis under sunlight, with Ag-deposited ($MgTiO_3$) photocatalyst are depicted below:

$$Ag + hv \rightarrow Ag\ (h^+ + e^-) \quad (5)$$

$$MgTiO_3 + hv \rightarrow MgTiO_3\ (h^+ + e^-) \quad (6)$$

$$Ag\ (e\text{-}) + MgTiO_3 \rightarrow MgTiO_3\ (e^-) + Ag \quad (7)$$

$$MgTiO_3\ (e\text{-}) + O_2 \rightarrow MgTiO_3 + {}^{\bullet}O_2^- \quad (8)$$

$$Ag\ (e\text{-}) + O_2 \rightarrow Ag + {}^{\bullet}O_2^- \quad (9)$$

$${}^{\bullet}O_2^- + H^+ \rightarrow {}^{\bullet}OOH \quad (10)$$

$$2\,{}^{\bullet}OOH \rightarrow O_2 + H_2O_2 \quad (11)$$

$$H_2O_2 + (e\text{-}) \rightarrow {}^{\bullet}OH + {}^-OH \quad (12)$$

$$Ag\ (h^+) + {}^-OH \rightarrow {}^{\bullet}OH \quad (13)$$

$$MgTiO_3\ (h^+) + {}^-OH \rightarrow {}^{\bullet}OH \quad (14)$$

$${}^{\bullet}O_2^-/\ {}^{\bullet}OH + Fuc \rightarrow CO_2 + H_2O + \text{degradation products} \quad (15)$$

This transport mechanism in the metal-loaded photocatalyst is anticipated to reduce charge carrier recombination, greatly enhancing photocatalytic performance.

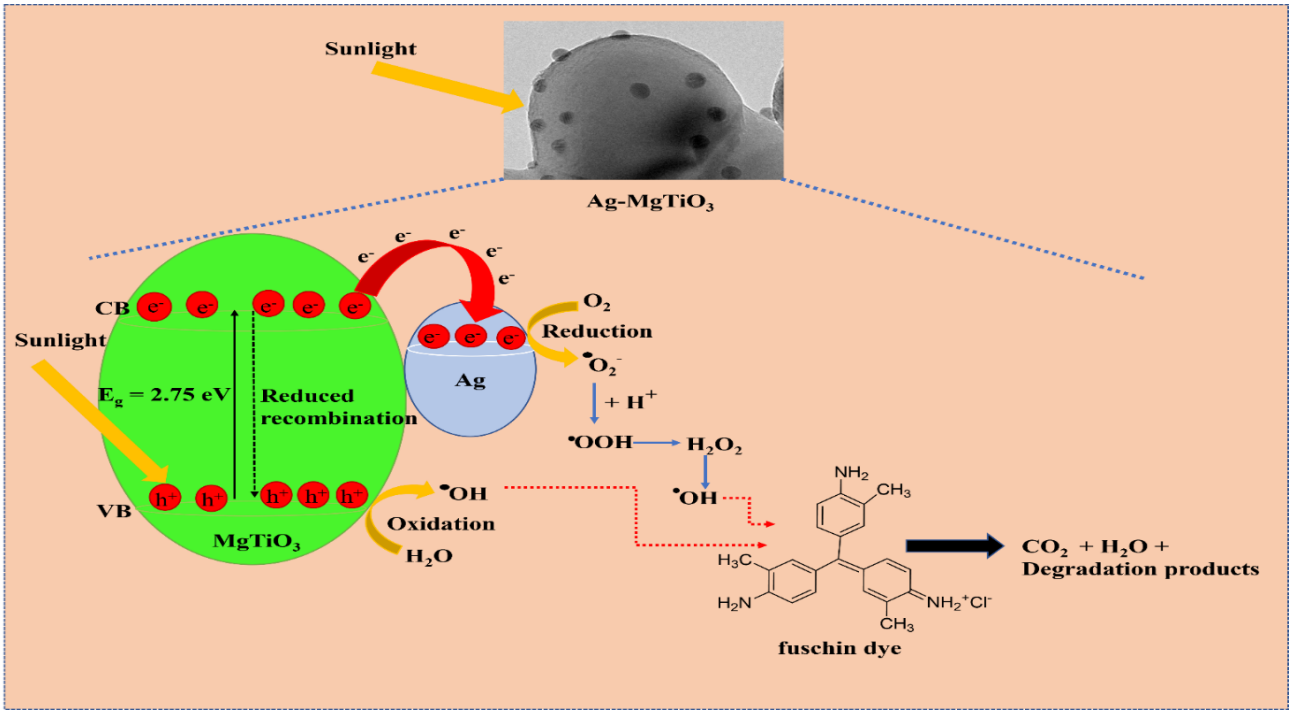

Scheme 3: Plausible mechanism of Fuchsin dye degradation under sunlight irradiation.

3.12 Photodegradation of textile dye in wastewater And Recyclability Studies

In practical applications, the reusability and stability of photocatalysts are essential for their effectiveness. To evaluate these aspects, a series of recycling tests were performed using an Ag-MgTiO3 composite to degrade Fuc dye. This involved running five sequential cycles, each with a 50-minute reaction duration. For each cycle after the initial one, the photocatalyst was retrieved via centrifugation, cleaned, and dried for subsequent use. According to Figure 13(a), the degradation efficiency of the Fuc dye dropped by just 17.4% from the first to the fifth cycle, demonstrating the high reusability of the Ag-MgTiO3 catalyst. The reduction in performance from 99.2% to 81.8% is likely due to some catalyst loss during the separation and recycling phases. In summary, the Ag-MgTiO3 composite shows excellent degradation performance, good renewability, and robust photostability, making it a highly effective material for photocatalytic applications. Fig 13(b) shows the photocatalytic efficiency of the produced materials Ag-$MgTiO_3$, which was tested using textile wastewater that we took from a textile dyer in Model Town, Degradation. The photocatalytic process was carried out under direct sunlight. 5 mg of photocatalyst was dispersed into 10 mL of textile wastewater at a 0.5 g/L concentration. Before irradiation, the suspensions were agitated in the absence of light for 30 minutes to establish an Equilibrium of adsorption and desorption processes between the dye molecules and the catalyst's surface. To initiate deterioration, the solution was stirred for 110 minutes with the vessel horizontal and exposed to direct sunlight. After removing the $MgTiO_3$ catalyst, roughly 5–6 mL of the solution was taken out and examined with a UV-visible spectrophotometer. The Ag-$MgTiO_3$ nanocomposite showed a markedly greater decline after 110 minutes of sunlight irradiation(99.4%).

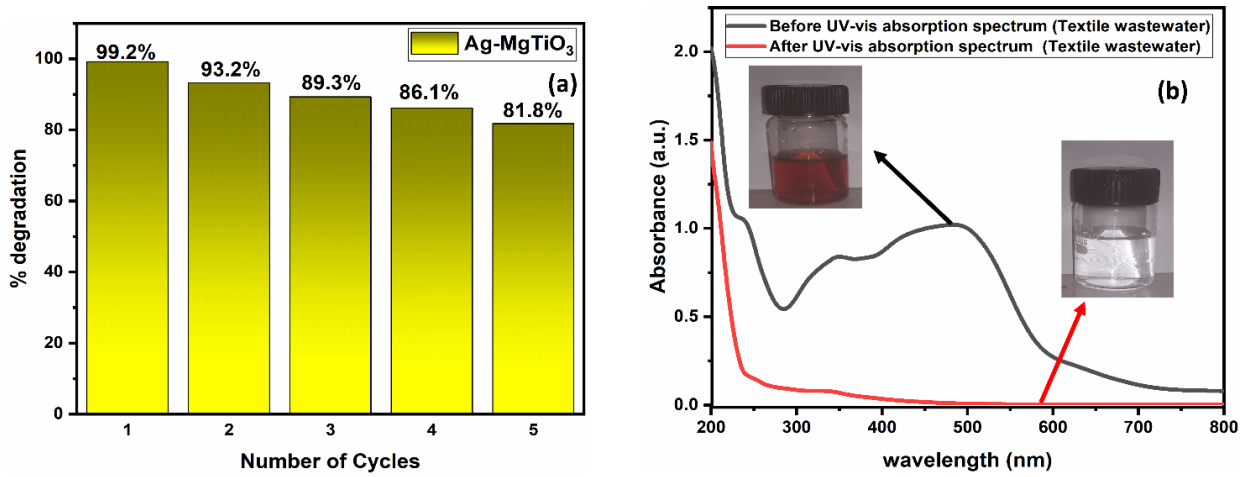

Fig.13:(a) Reusability studies,**(b)** degradation efficiency of the textile wastewater solution over Ag-$MgTiO_3$ photocatalyst when exposed to direct sunlight.

4. CONCLUSION

The sonochemical method was used to synthesize $MgTiO_3$ and enhance its photocatalytic properties by loading it with Ag metal. The effective fabrication of the samples was confirmed using various analytical techniques, including XPS, DRS, FE-SEM, EDS, HR-TEM, XRD, PL, and BET analyses. FE-SEM and HR-TEM images revealed that Ag was effectively deposited onto the $MgTiO_3$ surface in the form of small spheres. The photocatalytic efficiency of the synthesized samples was evaluated by examining the deterioration of Fuc dye under natural sunlight. Ag-MgTiO3 showed the highest photocatalytic efficiency and rate constant among the photocatalysts produced. PL, BET, and UV-visible DRS analyses showed that the composite effectively decomposed contaminants under natural sunlight thanks to its lower reformation rate, large surface area, and suitable band gap. The study also explored various factors affecting photocatalytic degradation, including catalyst concentration, pH levels, reaction kinetics, light sources, scavenger analysis, and the reusability of the catalyst. Trapping experiments identified h^+ as the main species driving pollutant degradation. The composite exhibited excellent recyclability over five cycles, with a high total organic carbon (TOC) removal rate, highlighting its efficiency and superiority over conventional physicochemical methods. HRMS study was conducted to identify the products and intermediates formed during the photodegradation. In conclusion, the Ag-$MgTiO_3$ catalyst revealed effective organic pollutant deterioration with sparse usage in natural sunlight, making it an attractive option for large-scale industrial wastewater treatment due to its cost-effectiveness, simplicity, and environmental benefits.

REFERENCES

[1] A. Akhundi, A. Habibi-Yangjeh, M. Abitorabi, S. Rahim Pouran, Review on photocatalytic conversion of carbon dioxide to value-added compounds and renewable fuels by graphitic carbon nitride-based photocatalysts, Catal. Rev. - Sci. Eng. 61 (2019) 595–628. https://doi.org/10.1080/01614940.2019.1654224.

[2] A. Sharma, S. Pahwa, S. Bhati, P. Kudeshia, Spanlastics: a Modern Approach for Nanovesicular Drug Delivery System, Int. J. Pharm. Sci. Res. 11 (2020) 1057. https://doi.org/10.13040/IJPSR.0975-8232.11(3).1057-65.

[3] R. Zhang, Y. Ai, Z. Lu, Application of Multifunctional Layered Double Hydroxides for Removing Environmental Pollutants: Recent Experimental and Theoretical Progress, J. Environ. Chem. Eng. 8 (2020) 103908. https://doi.org/10.1016/j.jece.2020.103908.

[4] V. Srivastava, E.N. Zare, P. Makvandi, X. qi Zheng, S. Iftekhar, A. Wu, V.V.T. Padil, B. Mokhtari, R.S. Varma, F.R. Tay, M. Sillanpaa, Cytotoxic aquatic pollutants and their removal

by nanocomposite-based sorbents, Chemosphere 258 (2020) 127324. https://doi.org/10.1016/j.chemosphere.2020.127324.

[5] MS Muthu, S.S. John, P. Ajith, D.P. Anand, Materials Today : Proceedings Preparation and characterization studies of nano graphene oxide, Mater. Today Proc. 66 (2022) 2449–2454. https://doi.org/10.1016/j.matpr.2022.06.367.

[6] D. Monga, S. Basu, Enhanced photocatalytic degradation of industrial dye by g-C 3 N 4 /TiO 2 nanocomposite: Role of shape of TiO_2, Adv. Powder Technol. 30 (2019) 1089–1098. https://doi.org/10.1016/j.apt.2019.03.004.

[7] D. Malwal, P. Gopinath, Enhanced photocatalytic activity of hierarchical three dimensional metal oxide@CuO nanostructures towards the degradation of Congo red dye under solar radiation, Catal. Sci. Technol. 6 (2016) 4458–4472. https://doi.org/10.1039/c6cy00128a.

[8] E.T. Soares, M.A. Lansarin, C.C. Moro, A study of process variables for the photocatalytic degradation of rhodamine B, Brazilian J. Chem. Eng. 24 (2007) 29–36. https://doi.org/10.1590/S0104-66322007000100003.

[9] A. Kumar, A. Kumar, V. Krishnan, Perovskite Oxide Based Materials for Energy and Environment-Oriented Photocatalysis, ACS Catal. 10 (2020) 10253–10315. https://doi.org/10.1021/acscatal.0c02947.

[10] P. Kanhere, Z. Chen, A review on visible light active perovskite-based photocatalysts, Molecules 19 (2014) 19995–20022. https://doi.org/10.3390/molecules191219995.

[11] T.P. Nguyen, Q.B. Tran, Q.V. Ly, L. Thanh Hai, D.T. Le, M.B. Tran, T.T.T. Ho, X.C. Nguyen, M. Shokouhimehr, D.V.N. Vo, S.S. Lam, H.T. Do, S.Y. Kim, T. Van Tung, Q. Van Le, Enhanced visible photocatalytic degradation of diclofen over N-doped TiO_2 assisted with H_2O_2: A kinetic and pathway study, Arab. J. Chem. 13 (2020) 8361–8371. https://doi.org/10.1016/j.arabjc.2020.05.023.

[12] M. Kurian, Advanced oxidation processes and nanomaterials -a review, Clean. Eng. Technol. 2 (2021) 100090. https://doi.org/10.1016/j.clet.2021.100090.

[13] M. Passi, B. Pal, A review on $CaTiO_3$ photocatalyst: Activity enhancement methods and photocatalytic applications, Powder Technol. 388 (2021) 274–304. https://doi.org/10.1016/j.powtec.2021.04.056.

[14] T. Puangpetch, P. Sommakettarin, S. Chavadej, T. Sreethawong, Hydrogen production from

water splitting over Eosin Y-sensitized mesoporous-assembled perovskite titanate nanocrystal photocatalysts under visible light irradiation, Int. J. Hydrogen Energy 35 (2010) 12428–12442. https://doi.org/10.1016/j.ijhydene.2010.08.138.

[15] U.O. Bhagwat, J.J. Wu, A.M. Asiri, S. Anandan, Synthesis of $MgTiO_3$ Nanoparticles for Photocatalytic Applications, ChemistrySelect 4 (2019) 788–796. https://doi.org/10.1002/slct.201803583.

[16] J. Yang, A. Mao, Z. Yue, W. Zhu, X. Luo, C. Zhu, Y. Xiao, J. Zhang, A simple base-mediated synthesis of diverse functionalized ring-fluorinated 4H-pyrans via double direct C-F substitutions, Chem. Commun. 51 (2015) 8326–8329. https://doi.org/10.1039/c5cc02073e.

[17] M.K. Suresh, J.K. Thomas, H. Sreemoolanadhan, C.N. George, A. John, S. Solomon, P.R.S. Wariar, J. Koshy, Synthesis of nanocrystalline magnesium titanate by an auto-igniting combustion technique and its structural, spectroscopic and dielectric properties, Mater. Res. Bull. 45 (2010) 761–765. https://doi.org/10.1016/j.materresbull.2010.03.019.

[18] E.A.V. Ferri, J.C. Sczancoski, L.S. Cavalcante, E.C. Paris, J.W.M. Espinosa, A.T. de Figueiredo, P.S. Pizani, V.R. Mastelaro, J.A. Varela, E. Longo, Photoluminescence behavior in $MgTiO_3$ powders with vacancy/distorted clusters and octahedral tilting, Mater. Chem. Phys. 117 (2009) 192–198. https://doi.org/10.1016/j.matchemphys.2009.05.042.

[19] S. Kumar Thatikonda, P. Gogoi, B. Kisan, A. Perumal, P. Sharma, P. Dobbidi, Magnetic properties of Co doped $MgTiO_3$ ceramics, Phys. B Condens. Matter 448 (2014) 330–332. https://doi.org/10.1016/j.physb.2014.02.054.

[20] C.Y. Teh, T.Y. Wu, J.C. Juan, An application of ultrasound technology in synthesis of titania-based photocatalyst for degrading pollutant, Chem. Eng. J. 317 (2017) 586–612. https://doi.org/10.1016/j.cej.2017.01.001.

[21] H.J. Jo, J.S. Kim, E.S. Kim, Microwave dielectric properties of $MgTiO_3$-based ceramics, Ceram. Int. 41 (2015) S530–S536. https://doi.org/10.1016/j.ceramint.2015.03.142.

[22] H. Wang, J.J. Zhu, J.M. Zhu, X.H. Liao, S. Xu, T. Ding, H.Y. Chen, Preparation of nanocrystalline ceria particles by sonochemical and microwave assisted heating methods, Phys. Chem. Chem. Phys. 4 (2002) 3794–3799. https://doi.org/10.1039/b201394k.

[23] A. Kumar, P. Choudhary, A. Kumar, P.H.C. Camargo, V. Krishnan, Recent Advances in Plasmonic Photocatalysis Based on TiO_2 and Noble Metal Nanoparticles for Energy Conversion , Environmental Remediation , and Organic Synthesis, (2021).

https://doi.org/10.1002/smll.202101638.

[24] Y.S. Fu, J. Li, J. Li, Metal/semiconductor nanocomposites for photocatalysis: Fundamentals, structures, applications and properties, Nanomaterials 9 (2019). https://doi.org/10.3390/nano9030359.

[25] A. Shawky, M. Alhaddad, K.S. Al-Namshah, R.M. Mohamed, N.S. Awwad, Synthesis of Pt-decorated $CaTiO_3$ nanocrystals for efficient photoconversion of nitrobenzene to aniline under visible light, J. Mol. Liq. 304 (2020) 112704. https://doi.org/10.1016/j.molliq.2020.112704.

[26] YZ. Zhen, J. Wang, J. Li, M. Fu, F. Fu, Y.Z. Zhang, J.H. Feng, Enhanced photocatalytic degradation for thiophene by Ag/α-MoO_3 heterojunction under visible-light irradiation, J. Mater. Sci. Mater. Electron. 29 (2018) 3672–3681. https://doi.org/10.1007/s10854-017-8298-z.

[27] K.H. Reddy, S. Martha, K.M. Parida, Erratic charge transfer dynamics of Au/$ZnTiO_3$ nanocomposites under UV and visible light irradiation and their related photocatalytic activities, Nanoscale 10 (2018) 18540–18554. https://doi.org/10.1039/c8nr06158k.

[28] 01-079-0831 $MgTiO_3$ jcpds.pdf, (n.d.).

[29] 04-0738 ag jcpds.pdf, (n.d.).

[30] C.H. Wang, X.P. Jing, W. Feng, J. Lu, Assignment of Raman-active vibrational modes of $MgTiO_3$, J. Appl. Phys. 104 (2008). https://doi.org/10.1063/1.2966717.

[31] B. Reynard, F. Guyot, High-temperature properties of geikielite ($MgTiO_3$-ilmenite) from high-temperature high-pressure Raman spectroscopy — Some implications for MgSiO3-ilmenite, Phys. Chem. Miner. 21 (1994) 441–450. https://doi.org/10.1007/BF00202274.

[32] R. Sánchez Zeferino, M. Barboza Flores, U. Pal, Photoluminescence and raman scattering in ag-doped zno nanoparticles, J. Appl. Phys. 109 (2011). https://doi.org/10.1063/1.3530631.

[33] S. Kaur, B. Pal, CO, (n.d.).

[34] J. Liqiang, Q. Yichun, W. Baiqi, L. Shudan, J. Baojiang, Y. Libin, F. Wei, F. Honggang, S. Jiazhong, Review of photoluminescence performance of nano-sized semiconductor materials and its relationships with photocatalytic activity, Sol. Energy Mater. Sol. Cells 90 (2006) 1773–1787. https://doi.org/10.1016/j.solmat.2005.11.007.

[35] M.K. Aulakh, B. Pal, Influence of co-catalyst amount/size for selective hydrogenation of 1,3-dinitrobenzene over Au-mTiO_2 nanocomposites under visible light, Adv. Powder Technol. 30

(2019) 1329–1337. https://doi.org/10.1016/j.apt.2019.04.008.

[36] J. Qin, H. Sun, S. Zhang, L. Yi, Y. Ruan, S. Wang, Z. Zhang, J. Wang, D. Fang, Investigation on the by-pass line orifice plate assisted hydrodynamic cavitation (B-PLOPA HC) degradation of basic fuchsin (BF) in wastewater, Sep. Purif. Technol. 287 (2022) 120501. https://doi.org/10.1016/j.seppur.2022.120501.

Plagiarism Report

turnitin

ORIGINALITY REPORT

15%	4%	14%	2%
SIMILARITY INDEX	INTERNET SOURCES	PUBLICATIONS	STUDENT PAPERS

PRIMARY SOURCES

1	Manjusha Passi, Bonamali Pal. "Design of a novel Ag-BaTiO3/GO ternary nanocomposite with enhanced visible-light driven photocatalytic performance towards mitigation of carcinogenic organic pollutants", Separation and Purification Technology, 2022 Publication	6%
2	Charu Maggu, Shelly Singla, Soumen Basu. "Unleashing the power of sunlight: Bi2O3/Sb2S3 photocatalysis for sustainable wastewater remediation of Tetracycline and Rhodamine-B", Journal of Environmental Management, 2024 Publication	3%
3	coek.info Internet Source	1%
4	Ujwala O. Bhagwat, Jerry J. Wu, Abdullah M. Asiri, Sambandam Anandan. " SynthesisofMgTiO NanoparticlesforPhotocatalyticApplications ", ChemistrySelect, 2019 Publication	1%
5	Muni Raj Maurya, Vijaykumar Toutam, Divi Haranath. "Comparative Study of Photoresponse from Vertically Grown ZnO Nanorod and Nanoflake Films", ACS Omega, 2017 Publication	<1%
6	Submitted to Deenbandhu Chhotu Ram University of Science and Technology Student Paper	<1%
7	Submitted to National Institute Of Technology, Tiruchirappalli Student Paper	<1%
8	Submitted to Visvesvaraya National Institute of Technology Student Paper	<1%
9	Bhavana Joshi, Edmund Samuel, Yongil Kim, Taegun Kim, Mohamed El-Newehy, Ali Aldalbahi, Sam S. Yoon. "Electrospun zinc-manganese bimetallic oxide carbon nanofibers as freestanding supercapacitor electrodes", International Journal of Energy Research, 2022 Publication	<1%

Siwari